

PRECISE ATOMIC MASS DETERMINATIONS WITH A
DOUBLE-FOCUSING MASS SPECTROMETER

PRECISE ATOMIC MASS DETERMINATIONS WITH A
DOUBLE-FOCUSING MASS SPECTROMETER

By

Neil Raymond Isenor, M.Sc.

A Thesis

Submitted to the Faculty of Graduate Studies

in Partial Fulfilment of the Requirements

for the Degree

Doctor of Philosophy

McMaster University

October 1959

DOCTOR OF PHILOSOPHY (1959)

McMaster University

(Physics)

Hamilton, Ontario

TITLE: Precise Atomic Mass Determinations with
a Double Focusing Mass Spectrometer

AUTHOR: Neil Raymond Isenor, B.Sc. (Acadia University)
M.Sc. (McMaster University)

SUPERVISOR: Professor H. E. Duckworth

NUMBER OF PAGES: viii, 52

SCOPE AND CONTENT:

A new large double-focusing mass spectrometer and its application to the determination of precise atomic mass values are described. A peak-matching technique is described by which mass difference values are obtained from voltage measurements.

The mass values obtained for Sr^{86} , Sr^{88} and Zr^{90} have largely resolved the discordance which had existed between the nuclear transmutation data and mass spectroscopic data in that region of the atomic mass table.

ACKNOWLEDGEMENTS

It is a pleasure to acknowledge the continued guidance and encouragement given by Professor H. E. Duckworth during the course of this investigation. I also thank Professor H. G. Thode and Dr. R. G. Summers-Gill for the advice rendered by them as members of my supervisory committee.

Much valuable assistance in the experimental work was given by Mr. R. C. Barber. Dr. J. T. Kerr and Dr. S. H. Ghoshal contributed valuable information and advice concerning the project.

Mr. Paul van Rookhuyzen and Mrs. Marion Tweedley have contributed much towards the preparation of the thesis.

Financial assistance, in the form of scholarships from the Ontario Research Foundation and the National Research Council of Canada, is gratefully acknowledged.

The expenses of the experimental work were met by research grants from the United States Air Force Office of Scientific Research and the National Research Council of Canada.

TABLE OF CONTENTS

	Page
INTRODUCTION	
1. Purposes of Atomic Mass Determination	1
2. Methods of Atomic Mass Determination	1
(i) Determination of Nuclear Reaction Q's	1
(ii) The Study of Pure Rotational Molecular Spectra ...	2
(iii) Mass Spectroscopic Methods	3
 CHAPTER I. MASS SPECTROSCOPIC METHODS OF ATOMIC MASS DETERMINATION	
1. Motion of Ions in Magnetic and Electric Fields	4
(i) Equations of Motion	4
(ii) Direction Focusing in Magnetic and Electric Fields	6
(iii) Velocity Focusing in Electric and Magnetic Field Combination	7
2. Modern Mass Spectroscopic Methods for the Determination of Atomic Masses	8
(i) Double-Focusing instruments	8
(ii) Resolution in Double-Focusing Instruments	9
(iii) The Cyclotron Resonance Mass Spectrometer.....	10
(iv) Parameters Used in Determination of Mass Differences	11
(v) The Doublet Method	12
(vi) Peak-Matching Method	12

CHAPTER II. EXPERIMENTAL

1. Geometry of Instrument	14
2. The Magnetic Field	16
3. The Electrostatic Analyser	19
4. The Ion Source	23
5. Beam Monitor System	25
6. The Collector	27
7. High Voltage Supply	29
8. The Voltage Flipping Circuits	30
9. The Vacuum System	32
10. Performance of the Instrument	33
(i) Previous Performance of Magnetic Analyser ...	33
(ii) Direction Focusing of Electrostatic Analyser	35
(iii) Performance of the Source and Various Beam Monitors	36
(iv) Velocity Focusing Check	36
(v) Acceleration Voltage Calculation and Check	37
(vi) Collection of Ions and Technique of Peak-Matching	37
(vii) Accuracy of Voltage Measurements	39
(viii) Resolution Attained	40

Table of Contents - Cont'd.

CHAPTER III. RESULTS OBTAINED AND DISCUSSION

1. Summary of Mass Difference Determinations	41
2. New Mass Values Directly Calculated from these Differences	42
3. Comparison with Mass Differences from Nuclear Reaction Data	43
(i) The Sr^{88} - Sr^{86} Mass Difference	45
(ii) The Zr^{90} - Sr^{88} Mass Difference	45
4. Other Mass Values Derived from This Investigation	48
CONCLUSIONS	49

<u>LIST OF FIGURES</u>	Page
1. Deflection of an Ion Beam in a Uniform Magnetic Field	5
2. " " " " " " " Radial Electric Field	5
3. General Scheme of the Apparatus	15
4. Entrance End of Magnet Analyser	17
5. Exit End of Magnetic Analyser	17
6. Block Diagram of Proton Resonance Magnetic Field Analyser	18
7. Electrodes and Fringe Blocks of Electrostatic Analyser	20
8. Pumping System of Electrostatic Analyser Vacuum Chamber	20
9. One Base of the Electrostatic Analyser	22
10. Source Arm of Electrostatic Analyser	22
11. Arrangement of Source Magnets	24
12. Cross-section of Ionization Region of Source	24
13. Source Voltage Supplies	26
14. Basic Scheme of Acceleration Voltage Supply	28
15. Electrostatic Analyser Modulation Circuit	31
16. Wave Form of Modulation Circuit	31
17. Block Diagram of Collection and Peak Display System	38
18. $H_2O - CO_2$ Doublet, Saw-Tooth Modulation Only	38
19. $N_2O - CO_2$ Doublet, Saw-tooth Plus Square Wave Modulation	38
20. $\frac{1}{2}(Zr^{90}Cl_2^{35}) - Kr$ Doublet, Saw-tooth Modulation Only	38
21. $\frac{1}{2}(Zr^{90}Cl_2^{35}) - Kr$ Doublet, Saw-tooth Plus Square Wave Modulation	38
22. Nuclidic Chart in the 50-Neutron Region Showing Reaction Q-Values	44

LIST OF TABLES

	Page
I. New Mass Differences	41
II. New Mass Values	43
III. Sr^{88} - Sr^{86} Mass Difference	45
IV. Zr^{90} - Sr^{88} Mass Difference	46
V. New Atomic Mass Values Resulting from this Work	50

INTRODUCTION

1. Purpose of Atomic Mass Determinations

The mass of a nuclide gives a measure of the energy which binds the nucleus together. This nuclear binding energy, usually expressed as a binding energy per nucleon, is of great importance in the development of a theory of nuclear structure. The variation in this energy with proton and neutron number gives evidence of exceptional stability for nuclei possessing certain numbers of each nucleon type, in agreement with the nuclear shell model. This model was an important step in the understanding of nuclear structure. From the great array of information regarding nuclear properties, it is hoped that ultimately the goal of understanding nuclear forces will be realized. Additions to this store of information will aid in the attainment of this goal.

The stability of nuclear species with respect to radioactive transmutation can be predicted, at least in part, from a knowledge of their masses. In particular, mass differences between adjacent isobars are important as they give the total energy available for beta decay. The threshold energy and energy release of a particle-induced nuclear reaction can also be computed from the relevant mass values.

2. Methods of Atomic Mass Determination

(1) Determination of Nuclear Reaction Q's. Particle-induced nuclear reactions usually take the form:



where A and B are the target and product atoms in their ground state, and X is the incident particle. Y is an emitted particle and is not always present. Q is the net energy change from the initial to the final states. Q is positive for energy released, and negative for energy absorbed. It is given by the mass difference $(X + A) - (B + Y)$.

In β -decay, the total energy release gives the mass difference between the parent and daughter atoms. Of course, a knowledge of the decay scheme is necessary to assign total decay energies.

If the mass differences obtained by the above means are to lead to atomic mass values, reference to a standard must be made. Oxygen-16 is the standard of atomic mass. One atomic mass unit is defined as one sixteenth of the mass of Oxygen-16. If atoms are to be assigned masses from transmutation data, they must be linked to O^{16} by a chain of transmutations, either induced or spontaneous. It is difficult to establish accurate mass values in the higher mass region by this method alone because of the errors accumulated along the reaction chains.

(ii) The Study of Pure Rotational Molecular Spectra. The moment of inertia of a linear molecule can be expressed very simply in terms of the masses of its atoms and their equilibrium separations. The rotational absorption frequencies of such molecules, which lie in the microwave region, depend on the isotopic species present in the molecule. These would be different, for example, for the molecule FCl^{35} than for the molecule FCl^{37} . From these frequencies, the ratio

of the mass of Cl^{35} to that of Cl^{37} can be calculated. In addition, a study of the rotational absorption spectra of symmetric-top molecules, yields ratios of mass differences. (Geschwind, Gunther-Mohr and Townes, 1954). This microwave spectra information is useful chiefly in checking other atomic mass data.

(iii) Mass Spectroscopic Methods. The masses of atoms can be determined by observing the deflections experienced by ions in certain combinations of electric and magnetic fields. In practice, mass differences, small compared with the masses of the ions being observed, are determined. With modern instruments, the accuracy of these mass difference determinations, among the light atoms, lies in the range 10^{-7} to 10^{-6} atomic mass units. This compares very favourably with nuclear reaction energy measurements, which are usually accurate to a few thousand electron-volts (10^{-6} AMU \approx 1 keV).

The mass spectroscopic method is very useful in establishing secondary standards in various regions of the mass table for use by nuclear disintegration investigators and by mass spectroscopists in determining other masses. The advantage of direct comparisons with standards is obvious; in general, such comparisons can be made only by the mass spectroscopists. Mass spectroscopic methods for the determination of atomic masses will be discussed in Chapter I.

CHAPTER I

MASS SPECTROSCOPIC METHODS OF ATOMIC MASS DETERMINATION

1. Motion of Ions in Magnetic and Electric Fields

(i) Equations of motion. In this section only fields commonly used in mass spectroscopy will be considered. These are

- (a) the homogeneous magnetic field, and
- (b) the radial electric field.

When an ion is allowed to enter a magnetic field, a force is exerted upon it proportional to the vector product of its velocity and the magnetic field vector \underline{B} . In the special case of an ion entering the field normal to the vector \underline{B} , the resulting force -- being normal to the velocity vector -- causes it to describe a circular path. The radius of curvature of this path is given by the relation

$$R = Mv/Be, \quad (1)$$

where v is the velocity of the ion and e/M its charge to mass ratio. That is, for ions carrying the same charge, the radii of curvature of their paths are directly proportional to their momenta. The deflection of ions of one particular momentum by a magnetic field is illustrated in Fig. 1.

The radial electrostatic field is commonly achieved by the use of two coaxial cylindrical electrodes. If an ion beam is allowed to enter such a device as shown in Fig. 2, those that

FIGURE 1

DEFLECTION OF AN ION BEAM IN A UNIFORM FIELD

One particular momentum component of an ion beam diverging from O, the object slit, will be focused at I, the image slit. The shaded area indicates the extent of the magnetic field, which is perpendicular to the paper.

FIGURE 2

DEFLECTION OF AN ION BEAM IN A RADIAL ELECTRIC FIELD

One particular energy component of an ion beam diverging from O will be focused at I. The radial field is established by a voltage applied across two cylindrical electrodes.

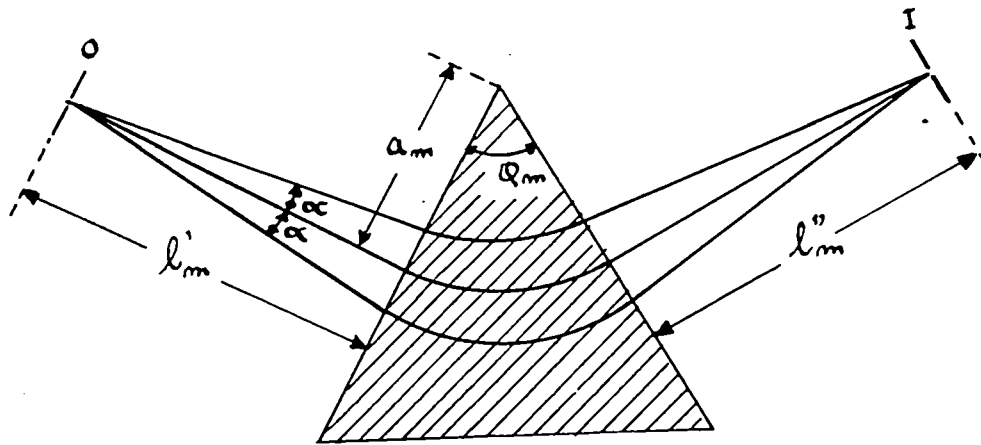


FIG. 1

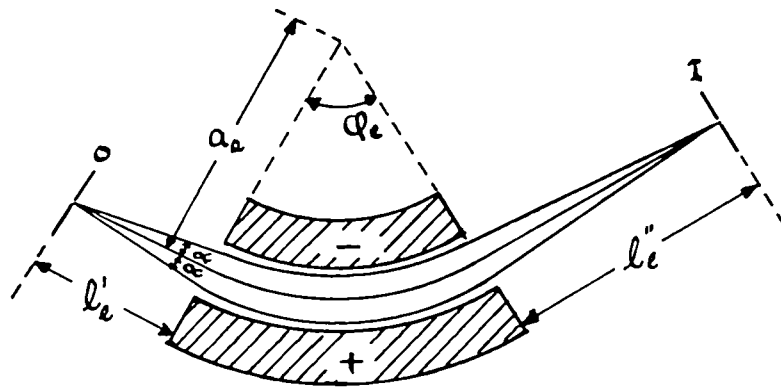


FIG. 2

follow the central path have energy given by the expression

$$Mv^2/R = \frac{Ve}{R \ln(R + \frac{1}{2}d)/(R - \frac{1}{2}d)} \quad \left. \vphantom{\frac{Ve}{R \ln(R + \frac{1}{2}d)/(R - \frac{1}{2}d)}} \right\} \quad (2)$$

or

$$Mv^2/2 = VeR/2d \quad \left. \vphantom{VeR/2d} \right\}$$

where R is the radius of the path taken by the ions while in the field established by the voltage V applied across the gap of width d. The electrostatic analyser is commonly used as a device for providing an ion beam of suitable energetic content to be analysed by a magnetic field.

(ii) Direction Focusing in Magnetic and Electric Fields.

The direction-focusing properties of homogeneous magnetic and radial electric fields have been analysed by Herzog (1934). The terminology used here in discussing focusing is that used by him. He showed that each of these cases could be treated as an optical combination of a prism (producing deflection) plus a cylindrical lens (producing focusing).

In Fig.1, an ion beam of a certain momentum is represented as diverging from O, with a half-angular spread of α . An ion with the median direction, after traversing a distance l'_m , enters the magnetic field normally, where it follows a circular path of radius a_m . After being deflected through an angle φ_m , it emerges from the field normally and continues to I, a distance l''_m , from the exit boundary of the field, where the ion beam is focused. A similar situation is represented in Fig.2, except that the beam is monoenergetic, and the deflecting field is a radial electric one.

The expression derived by Herzog for the focal length of the magnetic element is

$$f_m = a_m / \sin \varphi_m, \quad (3)$$

while that for the electric element is

$$f_e = a_e / \sqrt{2} \sin \sqrt{2} \varphi_e \quad (4)$$

For either case, the object and image distances, l' and l'' , are related by the equation

$$(l' - g)(l'' - g) = f^2 \quad (5)$$

where g , the distance from the field boundary to the principal focus, is given by

$$g_m = f_m \cos \varphi_m \quad (6)$$

for the magnetic case, and by

$$g_e = f_e \cos \sqrt{2} \varphi_e \quad (7)$$

for the electric case.

The fact that these fields focus ions with slightly divergent directions has been made use of to increase the intensity of ion beams in mass spectroscopes. It should be pointed out that this analysis of Herzog neglects terms containing α^2 and higher powers of α , and applies only for $\alpha \ll 1$.

(iii) Velocity Focusing in Electric and Magnetic Field Combinations. The mass spectrograph devised by F. W. Aston (1919) possessed a "velocity focusing" property. A beam of positive ions, after collimation, enters a uniform electric field, where it experiences a deflection through an angle θ . After leaving the

electric field, it enters a uniform magnetic field, and is deflected in the opposite direction through an angle greater than 2θ . The deflections experienced by the slower ions in each field is greater than that experienced by the faster ones. These fields are so arranged that the velocity dispersion produced by the first is cancelled by that of the second, with the result that ions of one particular mass, but a range of energies, are focused as a line on the photographic plate. This velocity-focusing property enabled Aston to use ion sources which produced ions with a wide energy spread (e.g., a gas discharge source).

2. Modern Mass Spectroscopic Methods for the Determination of Atomic Masses

(i) Double-focusing instruments. Instruments incorporating both velocity-focusing and direction-focusing principles were independently devised by Dempster (1935), Bainbridge and Jordan (1936), and Mattauch and Herzog (1934). These instruments employed sources such as the discharge source and the spark source, but gave greater precision than Aston's instrument because of the presence of direction-focusing. In such instruments, the image formed by the electrostatic focusing element serves as the object for the magnetic focusing element. The velocity dispersion produced by the first element is cancelled by that of the second, so that ions of one particular specific charge, but possessing initially

divergent direction, and a range of velocities, are brought to a focus.

In an electrostatic analyser the lateral displacement of the image caused by a velocity change from v to $v(1 + \beta)$, according to Herzog, is given by

$$b_e = a_e \beta \left(1 + \frac{f_e}{\rho'_e - \xi_e} \right), \quad (8)$$

the other terms having been previously defined. Similarly, in a magnetic analyser, the displacement of the image, caused by a similar velocity change, is

$$b_m = a_m \beta \left(1 + \frac{f_m}{\rho'_m - \xi_m} \right) \quad (9)$$

For two consecutive fields, placed so that the image of one serves as the object for the other, the total displacement would be given by the sum of these two terms. To achieve velocity focusing, the field must be arranged so that the two displacements are equal and opposite, that is

$$a_m \left(1 + \frac{f_m}{\rho'_m - \xi_m} \right) = a_e \left(1 + \frac{f_e}{\rho'_e - \xi_e} \right) \cdot \quad (10)$$

(ii) Resolution in double-focusing instruments. The resolution of an instrument such as outlined in the previous section can be shown to be

$$\frac{\Delta M}{M} = \frac{2S}{a_e} \frac{f_e / (\rho'_e - \xi_e)}{1 + f_e / (\rho'_e - \xi_e)} \quad (11)$$

where $\Delta M/M$ is the smallest fractional mass difference which can be resolved, and S is the sum of the widths of the initial and final defining slits. In the case of photographic detection, S is simply the width of the initial slit. It is seen from this equation that one should use narrow slits and large radii (hence large instruments) to achieve good resolution. The direction and velocity-focusing properties of double-focusing instruments enables one to employ small slits and still achieve useful ion intensities.

(iii) The Cyclotron Resonance Mass Spectrometer. The fact that a charged particle moving in a magnetic field normal to its motion describes a circular orbit with an orbital frequency dependent linearly on its specific charge has been exploited in the construction of the "mass synchrometer" of L. G. Smith (Smith, 1951; Smith and Damm, 1956). Ions diverge from a source and are brought to a perfect focus after traversing a complete circle. A first order focus occurs after a half circle is described. Here a radio-frequency modulator is placed which extracts a small amount of energy from the beam, causing it to miss the source upon the completion of the first orbit. In practice, several reductions of energy occur before the beam strikes the collector.

Since, for a given magnetic field, the specific charge is the only factor influencing the cyclotron frequency of ions

in the beam, for a given radio-frequency on the modulator, ions of only one particular specific charge will receive the correct energy reductions necessary to bring them to the collector.

Thus, one can obtain a mass spectrum by sweeping the applied frequency, and determine mass differences in terms of frequency differences.

(iv) Parameters Used in Determining Mass Differences. The specific charge of the ions which are transmitted by a magnetic analyser can be determined from a knowledge of the initial energy and the radius of the path taken. In instruments using photographic detection, the radius of the path is the variable parameter, the others being held fixed. Distances between lines on the plate can be measured, and mass differences calculated using the theoretical expression for M as a function of R . With instruments where an electrical collector, and hence a fixed path radius is used, mass differences can be determined by sweeping the magnetic field strength or the ion energy, and noting the values of those parameters which correspond with different mass spectral peaks.

In large double-focusing instruments, the trend is toward sweeping the ion energy as it enters the magnetic analyser. This is effected by sweeping both the acceleration voltage and the electrostatic analyser voltage. According to a theorem due to Blackney (1936), if all the electric fields experienced by the ion beam are changed in the ratio V'/V , then an ion beam of mass M' will travel the path formerly travelled by a beam of mass M , such that $M'/M = V/V'$.

In the cyclotron resonance mass spectrometer, the parameter varied in determining mass values is a frequency of the signal applied to the modulator. The relation between mass and frequency in this instrument is simply $M'/M = F/F'$.

(v) The Doublet Method. Although the dispersion law of an instrument may be known from theoretical considerations, it cannot usually be strictly relied upon over large mass ranges. This means that it is advisable to determine mass differences which are small compared with the mass of the ions being studied. These determinations are usually done by the "doublet" method. A doublet is a pair of mass-spectral lines or peaks whose specific charges almost coincide. One of the lines or peaks corresponds to the ions of unknown mass, while the other is a "standard." Quite often, multiply-charged ions are used as doublet members, since an ion of charge "ne" and mass number "A" will fall very near one of mass number "A/n." This enables one to determine the masses of the heavier isotopes, provided their mass numbers are integral multiples of the mass number of a standard. The mass differences reported in this thesis have been determined using the doublet method.

(vi) Peak-Matching Method. An important method of determining mass differences has grown out of the mass synchronometer of Smith. The peaks of a doublet are displayed on an oscilloscope by modulating the frequency of the signal with the same wave form used on

the horizontal plates of the oscilloscope. The amplified ion current is applied to the vertical plates. On alternate sweeps of the oscilloscope, the frequencies have the values F and $F + \Delta F$, so that the two doublet members of mass M and $M - \Delta M$ appear alternately on the screen. The two peaks are then carefully superimposed by adjusting the value of F . The mass difference, ΔM , can then be calculated from the relation:

$$\frac{M - \Delta M}{M} = \frac{F}{F + \Delta F}$$

A similar method has been developed (Quisenberry, Scolman and Nier, 1956) for use with a double-focusing mass spectrometer. In this case, the electric fields experienced by the ions are switched rapidly to display one and then the other doublet member on an oscilloscope. The mass difference is then found by carefully determining the switching voltage applied to the electrostatic analyser. The switching voltage applied to the source needs only to be approximately correct, since the instrument possesses velocity focusing. This method has also been used in obtaining the results reported in this thesis.

The advantages of this method are chiefly: (1) the peak positions relative to the dispersion parameter can be determined to a high degree of precision (about 1/1000 of a peak width), (2) drifts in the magnetic and electric fields can be tolerated, and (3) results of instrumental adjustment can be immediately seen on the oscilloscope screen. This makes adjustment and alignment of a large instrument a much less tedious task.

CHAPTER II

EXPERIMENTAL

1. Geometry of Instrument

The geometrical arrangement of the components of the mass spectrometer used in this investigation is shown in Fig. 3. It is a double-focusing arrangement using a 90° electrostatic analyser and a 180° magnetic analyser. The positions of the source and electric analyser with reference to the magnetic analyser are such that the object and image distances of the electrostatic analyser are equal. They are given by equation 5, which reduces to

$$l_e - g_e = f_c,$$

where $l_e' = l_e'' = l_e$. The magnetic analyser has $l_m' = l_m'' = 0$, since it is a 180° magnet. This follows from equations 3, 5 and 6, since $\theta_m = \pi$. The mean radius, a_m , of the beam path in the magnet is equal to a_e , the mean radius in the electrostatic analyser. The fact that this is a velocity-focusing arrangement can be verified by substituting the appropriate values into equation 10. The actual dimensions of the instrument are given in the caption to Fig. 3.

The slits shown in Fig. 3 serve the following purposes. S_1 is the principal slit or object slit. S_2 defines the angular divergence of the beam allowed to enter the electrostatic analyser. S_3 defines the energy range of the ion beam allowed to enter the magnetic analyser. Lastly, S_4 , the collector slit, selects the portion of the mass spectrum which is allowed to enter the collector.

FIGURE 3

GENERAL SCHEME OF THE APPARATUS

Dimensions

$$a_e = a_m = 107.5 \text{ in.}$$

$$\varphi_e = \pi/2 \text{ radians}$$

$$\varphi_m = \pi \text{ radians}$$

$$l_e' = l_e'' = 37.75 \text{ in.}$$

$$l_m' = l_m'' = 0$$

Slit Widths

$$S_1 = 0.0025 \text{ in.}$$

$$S_2 = 0.060 \text{ in.}$$

$$S_3 = \text{variable, usually } 0.05 \text{ in.}$$

$$S_4 = \text{variable, usually } 0.003 \text{ in.}$$

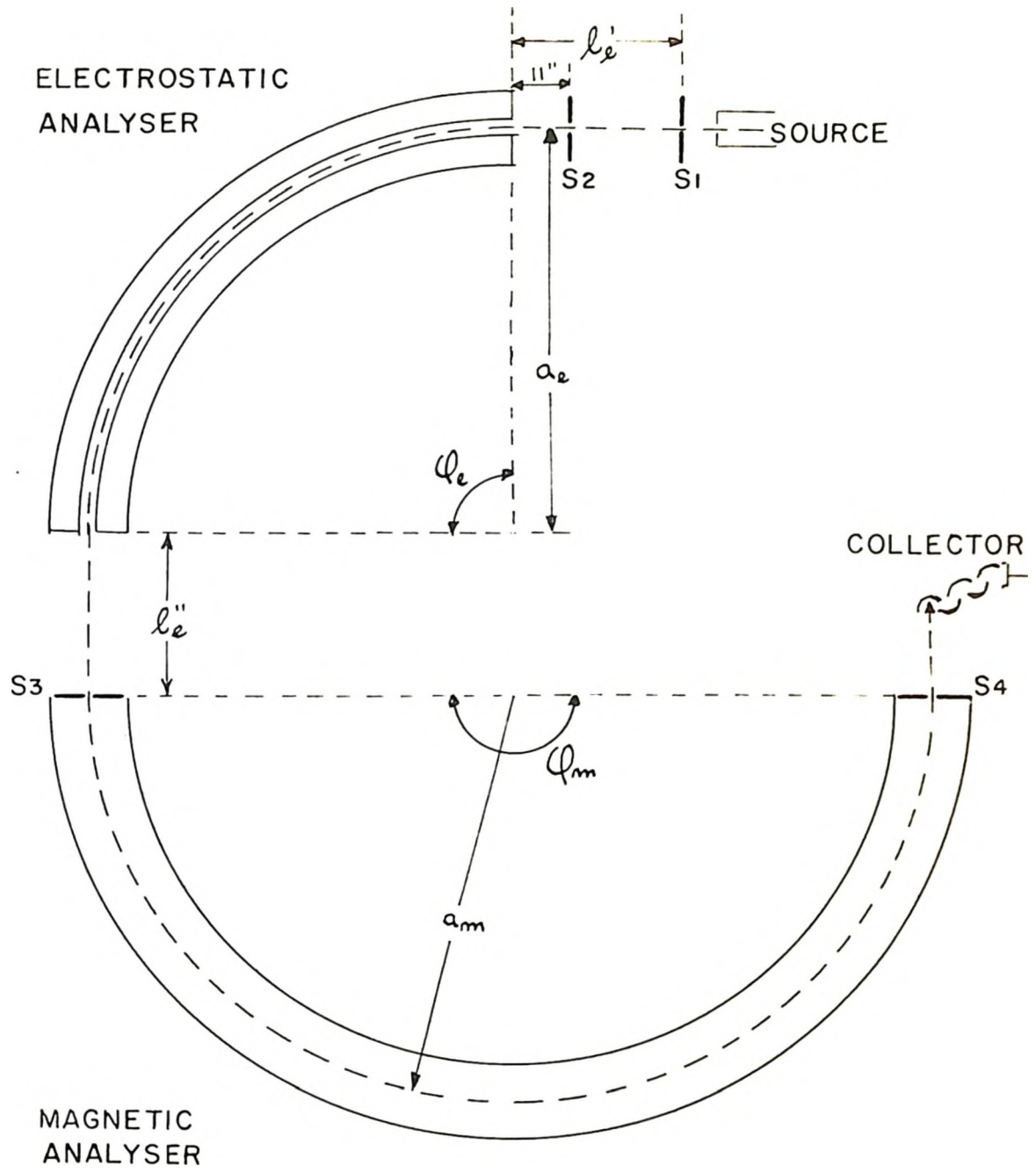


FIG. 3

2. The Magnetic Field

The magnet consists of 28 sections, each with its own coil, arranged to form a semicircle. The entrance and exit ends of the magnet are shown in Figs. 4 and 5. The gap between the magnet poles is 0.75 in. The field in this gap was originally made uniform by adjusting the pole pieces and the current in the coil of each section separately. The uniformity was checked by means of a proton resonance probe. This probe is now used to hold the magnetic field constant by means of an elaborate feed-back circuit, outlined in Fig.6. This circuit has been described in detail (Dewdney, 1955) and will be only briefly mentioned here.

The protons in a sample of mineral oil absorb radio frequency energy from a highly stable oscillator. The magnetic field is modulated in the vicinity of the probe by means of an audio frequency signal, which sweeps through the absorption signal at

400 cycles per second. The amplitude variations in the output of the oscillator are detected and fed back to control the magnet via an audio amplifier, a phase-sensitive rectifier, and a d-c amplifier. In this way, the magnetic field is held at a value determined by the frequency of the oscillator. The field can be swept slowly via a reversible motor which drives a trimming condenser in the oscillator. The approximate range over which the field can be controlled by this proton resonance device is from 500 to 1500 gauss.

FIGURE 4

ENTRANCE END OF MAGNETIC ANALYSER

The tube connecting the magnetic analyser to the electrostatic analyser is removed to show the adjustable slit (S_3 in Fig. 3). The coil on the end section of the magnet can be seen at the right. The proton resonance oscillator and probe are shown at the left.

FIGURE 5

EXIT END OF MAGNETIC ANALYSER

The cylindrical object connected to the flange at the end of the magnet is the electron multiplier. The micrometer adjustment for the collector slit (S_4 in Fig. 3) can be seen at the edge of the magnet gap. One pumping station of the magnetic analyser tube is seen at right, showing the mechanical and diffusion pumps and the liquid air traps.

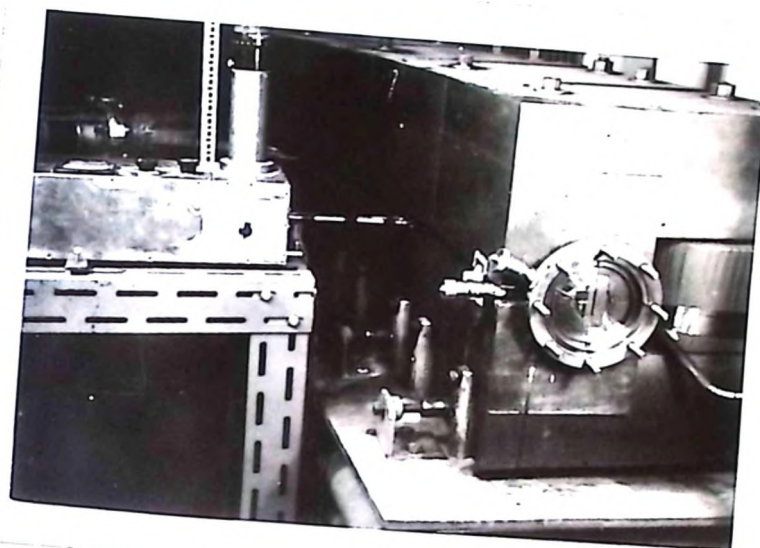


FIG. 4

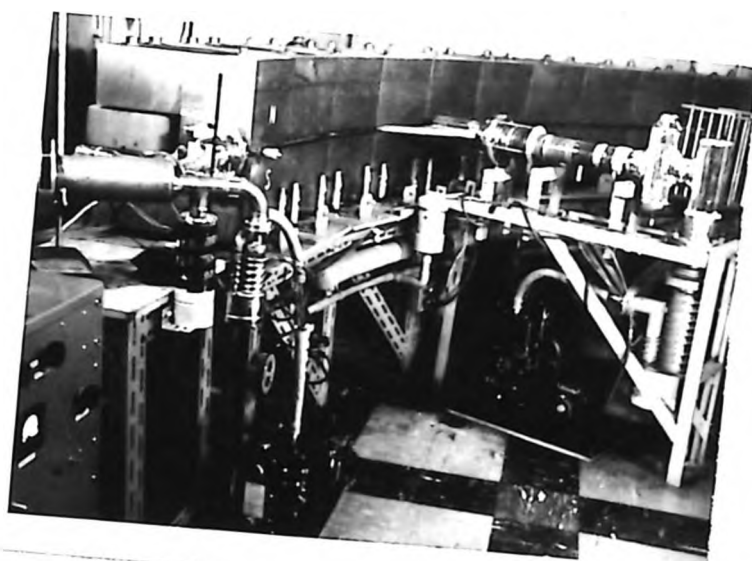


FIG. 5

FIGURE 6

BLOCK DIAGRAM OF THE PROTON RESONANCE MAGNETIC FIELD STABILIZER

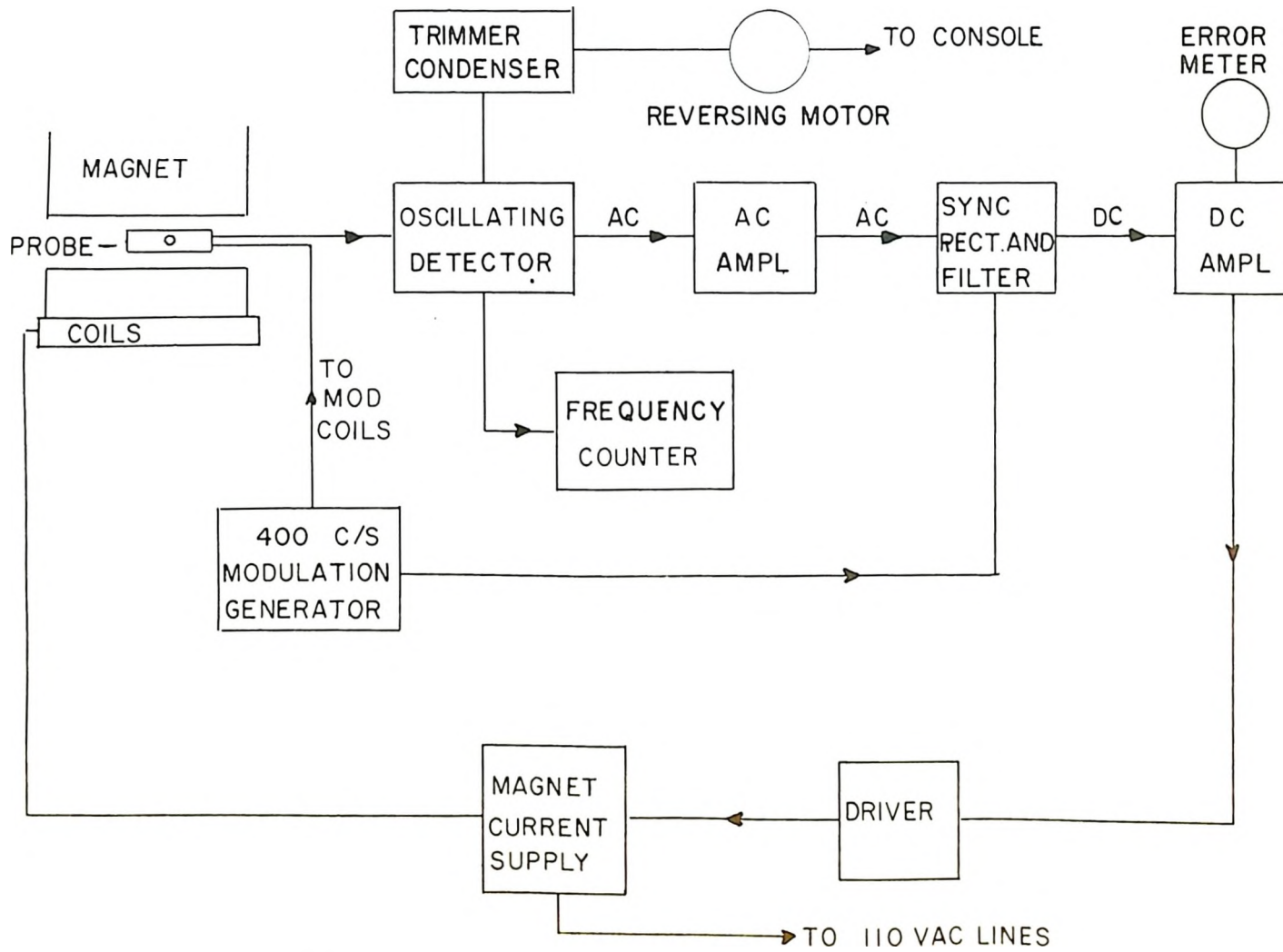


FIG. 6

3. The Electrostatic Analyser

The electrodes of the electrostatic analyser consist of gold-plated iron blocks, fitted together to form continuously - curved electrodes. The blocks are 6.5 inches high, 15 inches long and 3.5 inches thick. Each one rests on three alumina insulators, ground to a precise 0.625-inch thickness. The block faces were machined by bolting them in position to the steel base plate, and using a large vertical boring mill. The gap between the electrodes is an accurate 1.000 inches. The lining-up operation was done by means of a feeler gauge which used the accurately-machined inside edge of the steel base plate as a reference. Fig. 7 shows the electrodes, base plate and fringe blocks of the electrostatic analyser.

The blocks forming the electrodes of the electrostatic analyser were cut off so that they formed a 90° arc. The field is effectively terminated at the boundary of the electrodes by means of fringe blocks which are at ground potential. The positions and dimensions of these blocks were determined, using a graph due to Herzog (1935). The fringe block gap is 0.250 inches, and their separation from the ends of the electrodes is 0.255 inches.

The vacuum housing of the electrostatic analyser is made from 0.50-inch aluminum sheet, welded together to form a channel. This unit, fabricated for us by Aluminum Laboratories, Limited, sits on a neoprene rubber gasket on the steel base, and is

FIGURE 7

ELECTRODES AND FRINGE BLOCKS OF ELECTROSTATIC ANALYSER

Each electrode block sits on three alumina insulators, one of which can be seen. The small blocks on top of the electrode blocks ensure electrical continuity. The fringe blocks sit on the steel base plate and hence are at ground potential.

FIGURE 8

PUMPING SYSTEM OF THE ELECTROSTATIC ANALYSER VACUUM CHAMBER

This shows the vacuum housing of the electrostatic analyser with the pumping leads. The two diffusion pumps are backed by a single large mechanical pump. The diffusion pumps and traps are suspended from the analyser housing so that the whole will move on ball bearing supports.

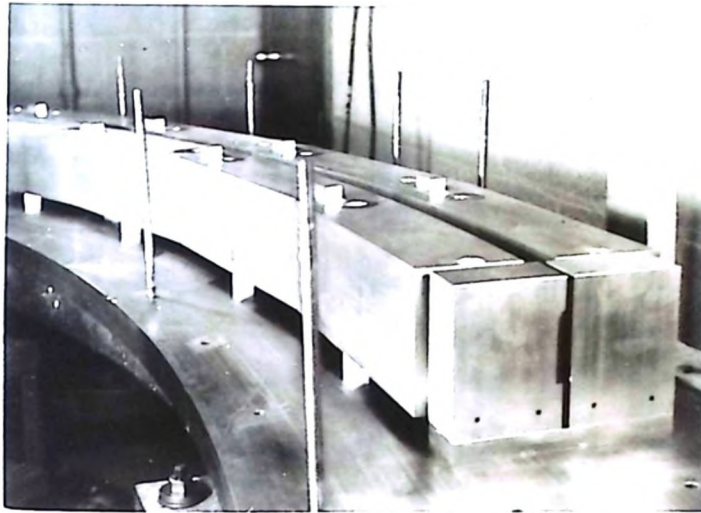


FIG. 7

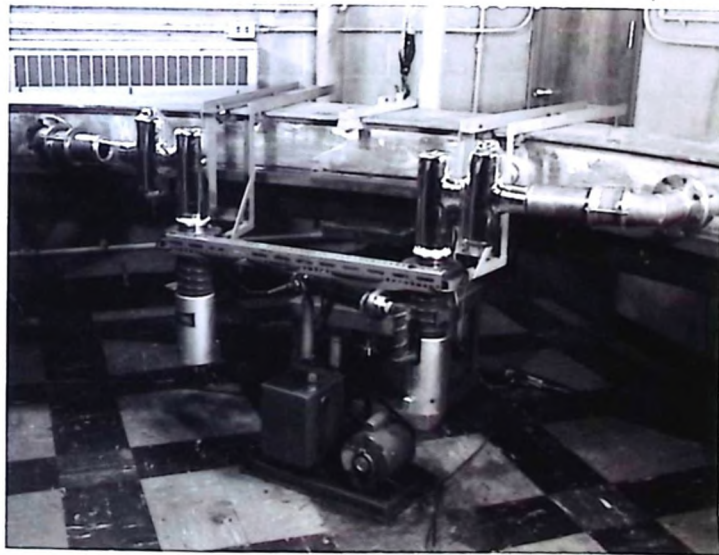


FIG. 8

clamped down by means of angle irons across its top. There are four ports in the housing, one where ions enter, one where ions leave, and two pumping ports on the side of the housing. Vacuum seals are made at these ports by means of neoprene "O" rings. The pumping ports and pumps are shown in Fig. 8.

The position of the electrostatic analyser with respect to the magnetic field is determined by three control arms, two of which are shown in Fig. 9. The ion exit point can be positioned via these arms, with respect to the magnet entrance slit. The other arm is at the source end of the analyser. The length of this arm can be adjusted to pivot the analyser about the ion exit point.

The analyser is supported by three 2-inch ball bearings. Each ball bearing sits on a platform which rests on a cluster of 1-inch ball bearings. The three-point suspension allows levelling of the analyser. The plates on which the clusters roll can be levelled individually by three jack screws. One of these suspension units is shown in Fig. 9. The whole analyser, which weighs about three tons, can be easily moved by hand on this suspension when it is not locked in position by the control arms.

The electrostatic analyser is connected to the magnetic analyser by means of a section of 3-inch copper pipe, which contains two bellows. The bellows allow some motion (~ 1 in.) of the analyser in the direction to and from the magnet, and also flex to allow transverse motion of the analyser.

FIGURE 9

ONE BASE OF THE ELECTROSTATIC ANALYSER

The analyser sits on three of these units, and can be locked in position by the control arms on the left. Each unit can be levelled separately by jack screws, and the three can then be brought to a common level by use of the same screws.

FIGURE 10

SOURCE ARM OF ELECTROSTATIC ANALYSER

The vacuum valve which isolates the source region is shown at center-left. The glass part is necessary for high voltage insulation. The micrometer is used to move the principal slit (S_1 in Fig. 3). One of the meters shown indicates total electron emission from the source filament. The other is for use with an electron bombardment crucible.

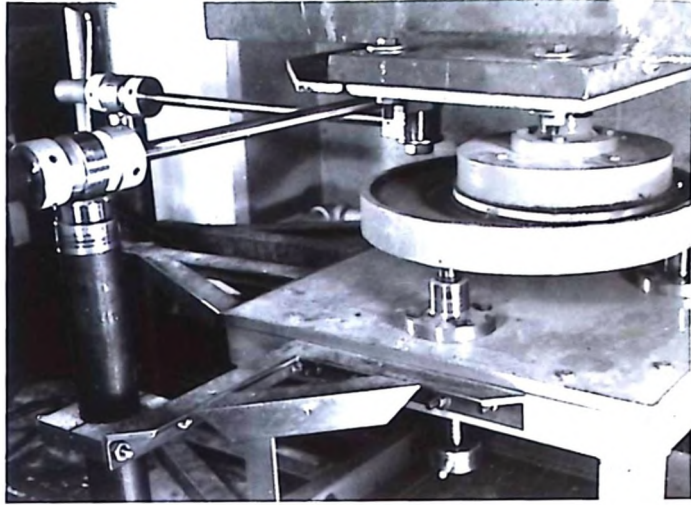


FIG. 9

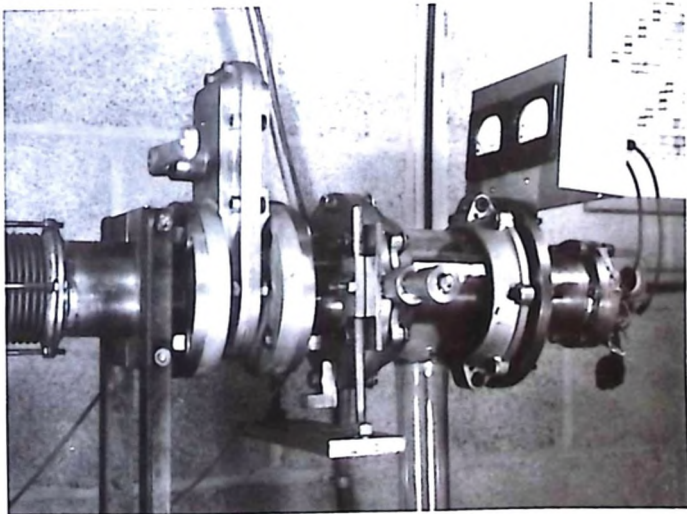


FIG. 10

The source of the mass spectrometer is connected to the electrostatic analyser by means of a 3-inch copper pipe containing two bellows. The source arm also contains a vacuum valve which allows the source to be removed without destroying the main vacuum. These parts are shown in Fig. 10. These bellows allow the source arm to be pivoted about S_2 in the horizontal and vertical directions, as well as allowing some longitudinal motion. In addition to this, the source, together with the plane containing the principal slit, S_1 , can be turned about horizontal and vertical axes with S_1 as the pivot. The source arm is supported by a channel iron frame which is fastened to the electrostatic analyser base plate and moves with it.

4. The Ion Source

The ion source, an electron bombardment source, is shown in Fig. 12. Electrons from the heated filament, D, are accelerated and enter a region where the substances to be ionized are present as gases. The ions which are formed are pushed toward the exit slit (shown at the bottom of Fig. 12) by a small positive voltage on the repeller, B. This source includes a crucible, C, which was added for vaporizing strontium. The crucible is heated by a filament, E, which is attached to its supports.

In order to constrain the electrons to move in a straight path across the ionization region, small magnets are located in the source, as shown in Fig. 11. With like poles together, and iron

FIGURE 11

ARRANGEMENT OF THE SOURCE MAGNETS

- A. Alnico magnets
- B. Iron pole pieces
- C. Ionization region
- D. Electron emission filament region
- E. Crucible region
- F. Non-magnetic retaining form

The magnets are arranged with like poles together to give a strong field in the ionization region. The slit in the ionization region is the ion exit slit.

FIGURE 12

CROSS-SECTION OF IONIZATION REGION OF SOURCE

- A. Mycalex insulator
- B. Ion repeller plate
- C. Crucible
- D. Electron emission filament
- E. Crucible heater filament
- F. Magnet pole pieces (B in Fig. 11)
- G. Gas inlet

The ionizing electrons travel from the filament toward the crucible, ionizing any gases which may be present. The repeller pushes the ions so formed toward the exit slit, where they leave the ionization region and enter the region where they are accelerated.

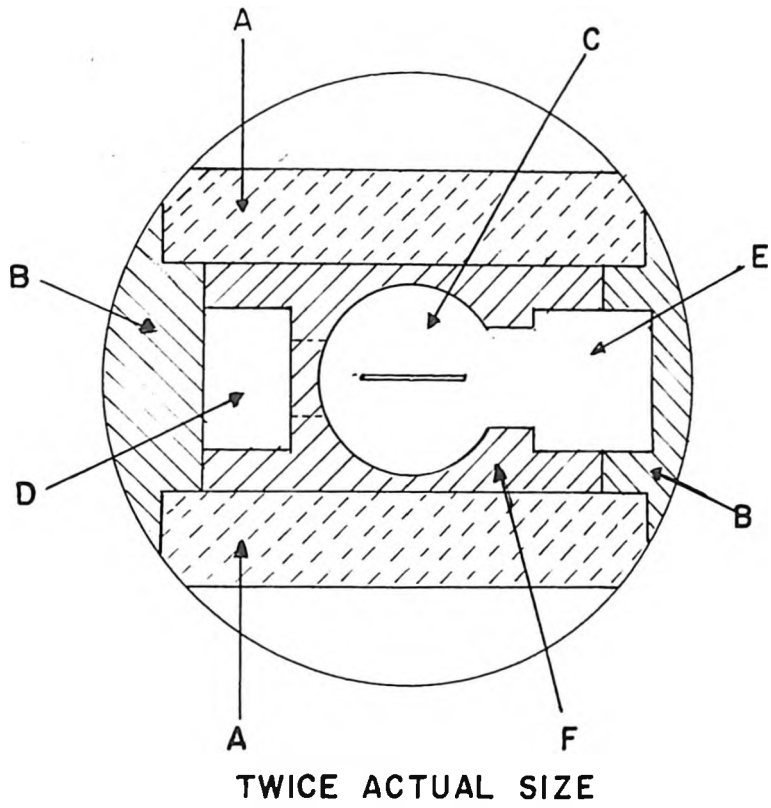


FIG. 11

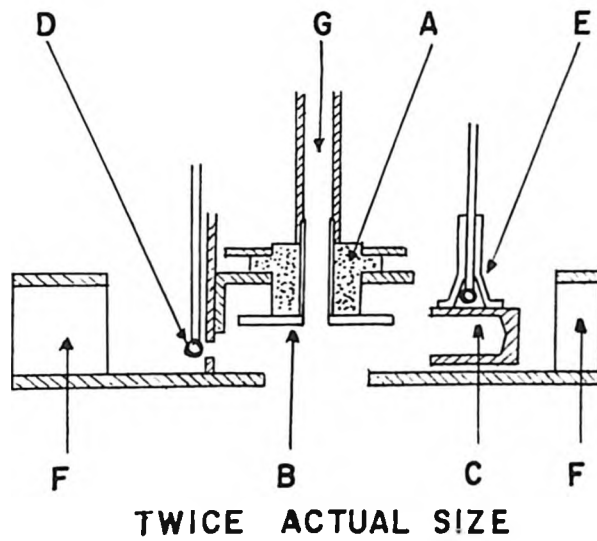


FIG. 12

armatures across their ends, the magnets produce a field in the ionization region, sufficient for this purpose.

To make possible the study of zirconium, the crucible shown in Fig. 12 was removed, and a glass tube was so positioned that its open end extended into the crucible region. The closed end of the tube contained zirconium tetrachloride, and was heated by means of a nichrome ribbon element.

Under normal operation, the voltage (with respect to the source housing) of the electron emission filament was -90 to -220 volts and of the repeller was +9 volts. In order to obtain $(\text{ZrCl}_2)^{++}$ ions, however, the filament voltage had to be lowered to -300 volts. The normal total emission current of the filament was about 5 milliamperes. The circuits for providing the source voltages are shown in Fig. 13.

5. Beam Monitor System

The first beam monitor is located just behind S_2 . This is a diaphragm which catches the top and bottom of the ion beam and so gives a measure of the ion current at this point. At the exit of the electrostatic analyser is a pair of collecting plates, one catching the bottom of the beam, and the other catching the top. They are 0.625 inches apart. Currents recorded here indicate when ions are passing through the analyser, and also help one to center

FIGURE 13

SOURCE VOLTAGE SUPPLIES

The isolation transformers and batteries are housed in an oil-filled tank, while the ΔV_a circuit sits in a lucite box supported by lucite rods.

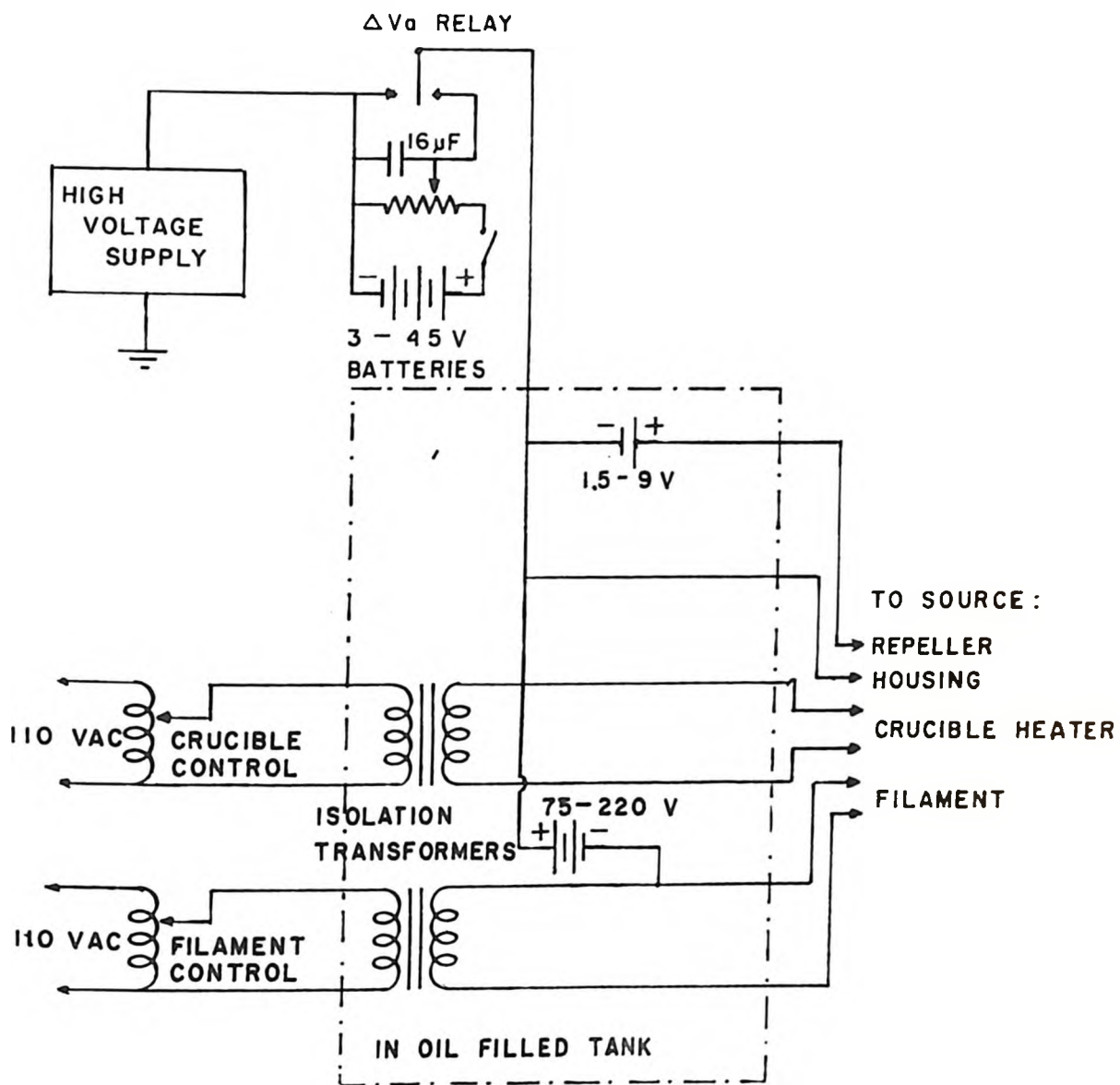


FIG. 13

the beam in the vertical direction. Behind S_3 is a Faraday cup which can be placed in a position to measure the entire beam current which enters the magnetic analyser. The current is normally checked at this point during operation of the instrument to permit adjustment of the source and the acceleration voltage.

The final beam monitor, the collector itself, is an electron multiplier. It detects that portion of the ion beam, now resolved into mass components, which leaves the magnetic analyser through S_4 .

6. The Collector

The collector, shown in Fig. 5, is an electron multiplier of the Allen type (Allen, 1947). There are 14 stages, the inter-stage voltage being about 400 volts. The gain of this multiplier is about 10^6 and appears to be quite constant. The signal from the multiplier can be displayed on an oscilloscope after passing through a very simple a-c amplifier. The arm connecting the multiplier to the magnetic analyser contains a bellows which allows the multiplier to be moved transversely so as to collect the maximum ion current. The position of the multiplier needs to be only roughly determined, since the entrance aperture is 0.25 inches wide.

FIGURE 1A

BASIC SCHEME OF ACCELERATION VOLTAGE SUPPLY

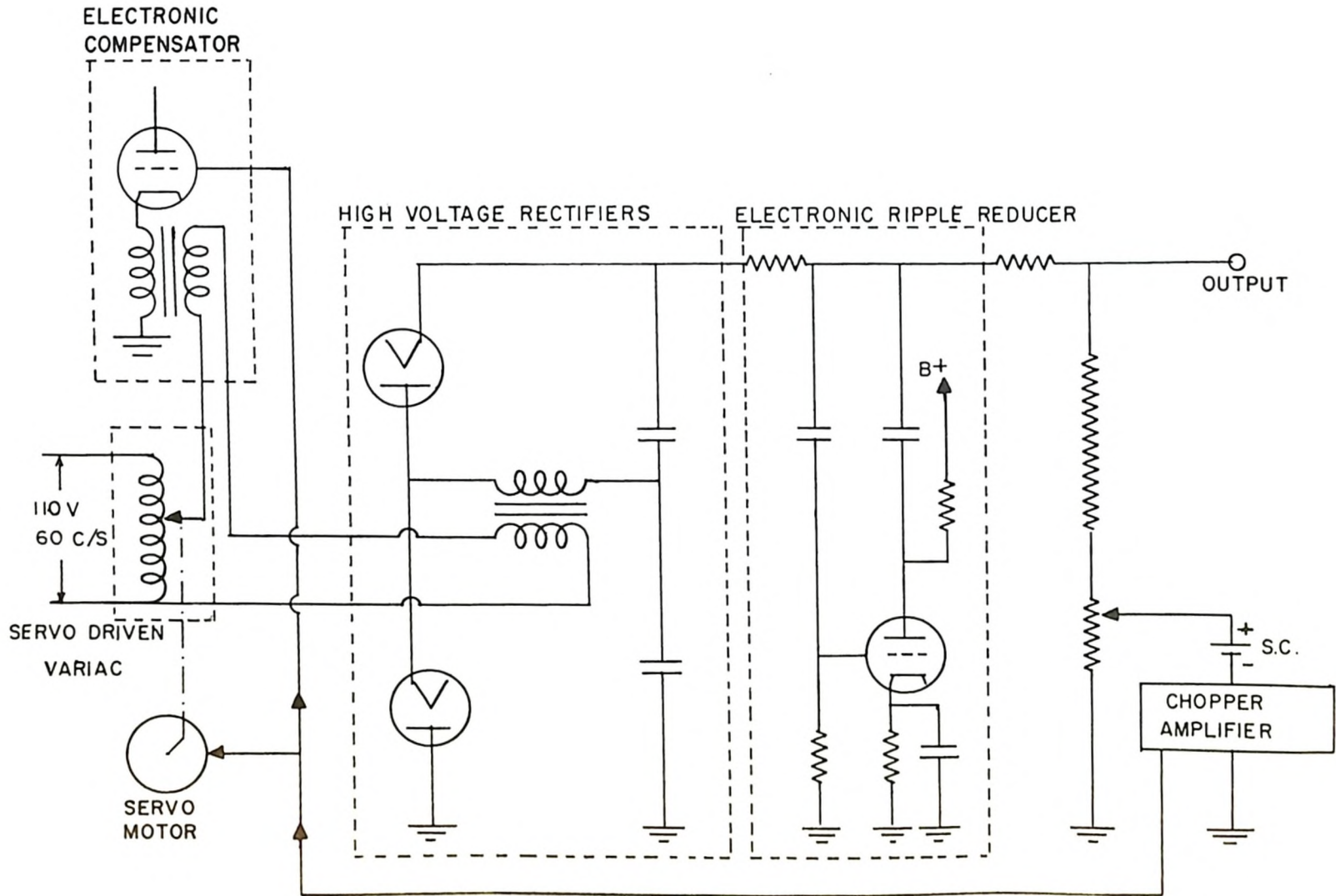


FIG. 14

8. The Voltage Flipping Circuits

The flipping voltage is applied to the electrostatic analyser electrodes and to the source by means of fast mercury-wetted contact relays. These relays (C.P. Clare Type HGP2004) are single-pole, double-throw types, with a break-before-make contact sequence. The maximum floating time is 0.001 second. The circuits which apply the flipping voltages can be seen in Fig. 13 and 15. The flipping voltage, ΔV_a , which is added to the acceleration voltage, is obtained from a potentiometer across three 45-volt batteries, while the flipping voltage, ΔV , which is added to the electrostatic analyser, is similarly obtained from two 1.35-volt mercury cells.

The relays of both circuits are driven by 30-cycle square waves obtained from scale-of-two circuits triggered by 60-cycle pulses from a Schmidt trigger circuit. The circuit which drives the ΔV_a relay, of course, must be at the potential of the source, that is, about 50 kilovolts above ground, and therefore its power must be supplied through isolation transformers. To accomplish this, two filament transformers (150 VA) are run back-to-back to achieve a 1:1 ratio and a total isolation rating of 50 kilovolts.

Connected also into the ΔV flipping circuit is a small transformer which applies a saw-tooth wave form (0 to ~ 1 volt) to the analyser electrodes. This saw-tooth comes from the sweep

FIGURE 15

ELECTROSTATIC ANALYSER MODULATION CIRCUIT

The modulation voltage is divided equally between the two electrostatic analyser electrodes by a potential divider.

FIGURE 16

WAVE FORM OF MODULATION CIRCUIT

This is the a-c component of the voltage across the analyser electrode. ΔV is the amplitude of the square wave component. The saw-tooth component serves to sweep the peaks linearly across the collector slit.

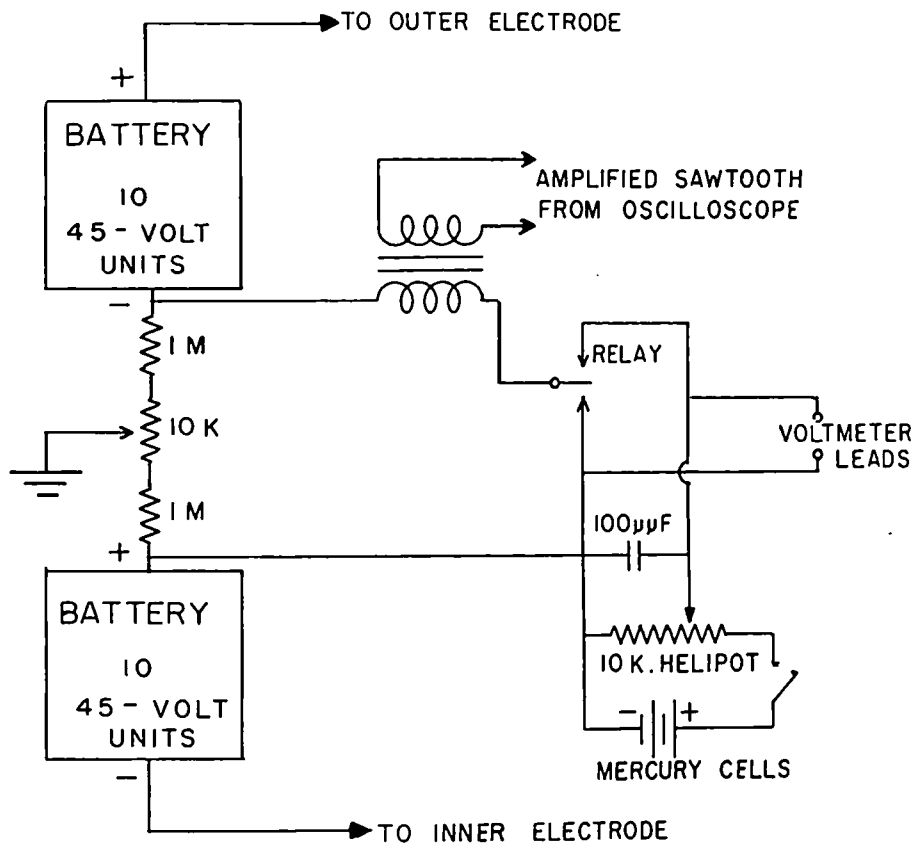


FIG. 15

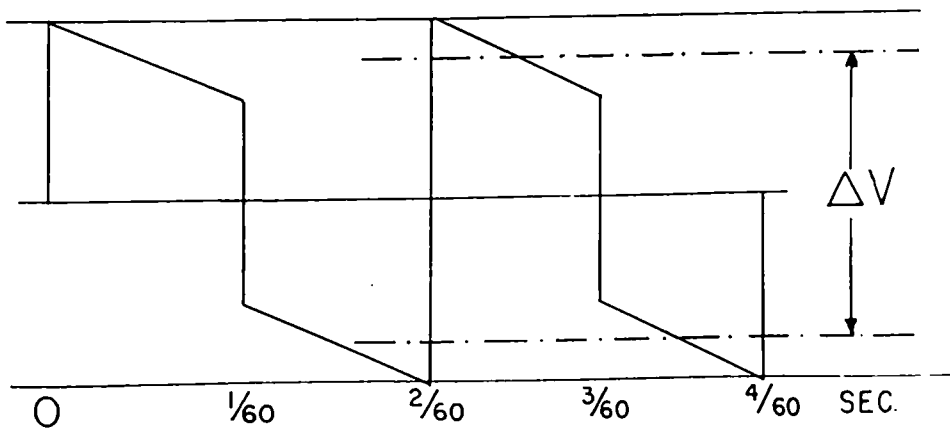


FIG. 16

voltage of the oscilloscope which is used to display the peaks which are received at the collector. Thus, the ion current is plotted on the oscilloscope as a function of the voltage on the electrostatic analyser. With a 60-cycle saw-tooth, properly phased with respect to the 30-cycle flipping voltage, the wave form modulating the electrostatic analyser is shown in Fig. 16.

The flipping voltage (ΔV_a), which is applied to the source to switch from one doublet member to the other, need not be critically determined because of the velocity focusing of the instrument. This voltage can be expressed simply as

$$\Delta V_a = V_a \Delta M/M,$$

where ΔM is the mass difference to be determined, and M is the mass value at which the determination is made. Thus, knowing V_a , ΔV_a can be calculated and set accurately enough, having only an approximate knowledge of the value of $\Delta M/M$.

9. The Vacuum System

The system is evacuated by five 4-inch oil diffusion pumps, and two smaller ones, backed by rotary pumps. Three of the larger pumps evacuate the copper tube which occupies the magnet gap, and two evacuate the electrostatic analyser housing. One of the pumping units of the magnetic analyser is shown in Fig. 5, while the pumps on the electrostatic analyser housing are shown in Fig. 8.

Each of these diffusion pumps is equipped with a liquid air trap. The two smaller diffusion pumps evacuate the source region and the electron multiplier region. The source region is well isolated from the rest of the system, so that gas can be introduced into it without raising the pressure in the analyser region.

The flanges on the magnetic analyser tube are fitted with aluminum gaskets, while those on the electrostatic analyser are fitted with neoprene "O" rings. A large flat neoprene gasket forms the seal between the aluminum housing of the electrostatic analyser and its steel base plate.

Under typical operating conditions pressures of $\sim 2 \times 10^{-6}$ mm Hg were obtained in the magnet region, while pressures in the electrostatic analyser ranged from 6 to 10×10^{-6} mm Hg. It is hoped that this figure will be improved with the help of a helium leak detector. The pressure in the electron multiplier was about 10^{-5} mm Hg, while that in the source region varied from 10^{-5} to 10^{-4} mm, depending on the rate at which gas was allowed to enter the source. At source pressures above 10^{-4} mm Hg, high voltage breakdown generally occurred.

10. Performance of the Instrument

(i) Previous Performance of Magnetic Analyser. The magnetic analyser was first used as a single-focusing mass spectrometer in 1955 by Dewdney. The resolution obtained was very close to that calculated from its dimensions. Mass differences were determined

at this time by sweeping the value of the magnetic field and thereby obtaining, on a chart-recorder, a mass spectrum.

Measurements were made of the distances between peaks on the chart, and mass differences were calculated from these measurements.

In 1957 Kerr used a different method for obtaining mass differences. He kept the magnetic field constant and changed the accelerating voltage to collect first one peak of a doublet, and then the other. This method avoided hysteresis effects in the magnet. In order to locate the top of a mass spectral peak, he modulated the accelerating voltage with a 60-cycle sine wave. This produced, at the collector, a signal which, when displayed on an oscilloscope, exhibited a symmetrical 120-cycle pattern when the accelerating voltage was such that the peak was exactly centered on the collector.

During recent experiments the ion path through the magnet was reversed. This was necessary in order to accommodate the energy analyser in the available space. The magnetic analyser was found to work satisfactorily during these experiments, after adjustments of the position of the electrostatic analyser were completed.

The performance of the proton resonance control circuit is somewhat erratic because of its great sensitivity. Fluctuations in the line voltage, discharges in the source, and other electrical disturbances are sufficient to cause sudden changes in the magnetic

field strength, with the result that the proton resonance circuit loses control. This circuit was found to work best during evenings and week-ends, when voltage fluctuations in the line were presumably less frequent. When the circuit was operating satisfactorily, it controlled the magnetic field to a high degree of precision, probably to better than 0.001%.

(ii) Direction Focusing of the Electrostatic Analyser. The source arm and the connecting arm to the magnetic analyser were made so that the object distance l'_e and the image distance l''_e were each equal to 37.75 in. to satisfy equation (5). The slit S_2 , of width 0.060 in., limits the divergence of the beam from the source to 0.0023 radians in the horizontal plane. This divergence is small enough to cause negligible broadening, due to the second order terms involving α , of the image at the entrance to the magnetic analyser. The actual beam width (for a repeller voltage of 9 volts) at the entrance of the magnet was 0.016 in. under good conditions, and can be attributed to an energy spread of 6.5 volts in the source with a source slit width of 0.0025 in.

A check on the direction-focusing of the electrostatic analyser was made by moving the slit S_2 laterally. When the source arm of the analyser was set at the wrong angle, the shape of the mass spectral peaks, obtained at the collector, changed when the slit was moved. When adjustment of the analyser was proper, the

peaks retained the same shape, simply dropping in intensity as the slit approached either extreme position.

(iii) The performance of the source and various beam monitors. The exit slit of the source is 0.5 in. from the disk containing S_1 . The acceleration voltage is applied across this gap. S_1 can be moved laterally in order to align it with the source slit. The ion beam passing through this slit spreads to a width of ~ 0.25 in. on arriving at S_2 . The diaphragm behind S_2 collects about 10% of the total beam current. Currents of $\sim 10^{-9}$ ampere were usually collected here, which meant that the total current beam was $\sim 10^{-8}$ ampere in typical operation.

The current collected at the entrance to the magnetic analyser, behind S_3 , was usually about 5×10^{-11} ampere. After this beam was resolved into its various mass components, currents detected at the final collector ranged from 10^{-12} to 10^{-15} ampere, depending upon the substance being introduced into the source. The electron multiplier, with a gain of $\sim 10^6$, gave currents of 10^{-6} to 10^{-9} ampere for such mass spectral peaks.

(iv) Velocity Focusing Check. By applying some flipping voltage to the source, while applying a saw-tooth sweep to the electrostatic analyser field, the velocity focusing property of the instrument is easily checked. If velocity-focusing is not satisfactory, a mass spectral peak appears as a double trace on the oscilloscope screen. It was found that when the source arm

and position of the electrostatic analyser were adjusted to give proper direction-focusing, good velocity focusing also resulted.

(v) Acceleration voltage calculation and check. The values of the resistors in the high voltage precision chain were determined by Kerr (1957). This knowledge enables one to determine the acceleration voltage by measuring that across the standard 1000-ohm resistor at the base of the chain. When all adjustments were made to give direction and velocity-focusing, the acceleration voltage required to pass an ion beam through the electrostatic analyser was determined to be 50717 volts. From the geometry of the electrostatic analyser and a knowledge of the voltage across the electrodes, one can calculate a value for the acceleration voltage required to pass ions through it. This value was calculated to be 50915 volts. This difference of 0.4% could be caused by the position of the object or image slit being transversely displaced from the proper position by 0.43 in. Such a displacement in an instrument of this size should not affect the performance in a noticeable way.

(vi) Collection of ions and technique of peak-matching.

Figure 17 shows a block diagram of the circuit which amplifies the ion current and displays it as mass-spectral peaks on an oscilloscope. Due to the wave form (Fig.16) which is applied to the electrostatic analyser, one doublet member and then the other

FIGURE 17

BLOCK DIAGRAM OF COLLECTION AND PEAK DISPLAY SYSTEM

This circuit translates ion current into peaks on an oscilloscope. A pattern such as that on the oscilloscope in this figure indicates proper adjustment of the electrostatic analyser modulation voltage.

FIGURE 18

$N_2O - CO_2$ DOUBLET, SAW-TOOTH MODULATION ONLY

FIGURE 19

$N_2O - CO_2$ DOUBLET, SAW-TOOTH PLUS SQUARE WAVE MODULATION

FIGURE 20

$1/2(Zr^{90}Cl_2^{35}) - Kr^{80}$ DOUBLET, SAW-TOOTH MODULATION ONLY

FIGURE 21

$1/2(Zr^{90}Cl_2^{35}) - Kr^{90}$ DOUBLET, SAW-TOOTH PLUS SQUARE WAVE MODULATION

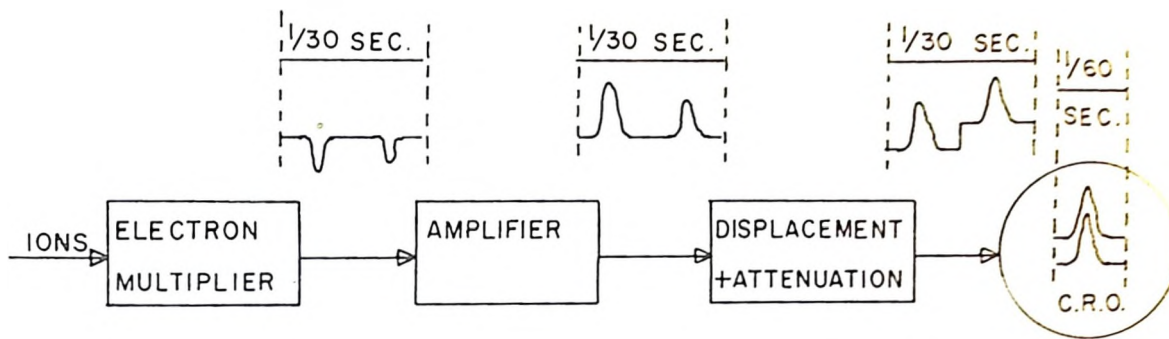


FIG. 17

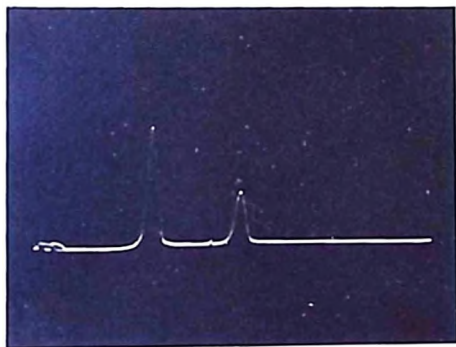


FIG. 18

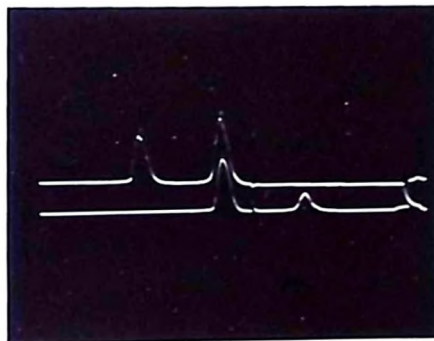


FIG. 19

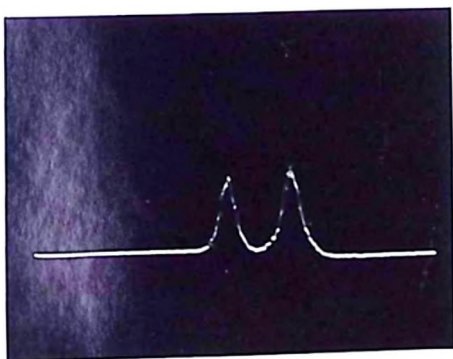


FIG. 20

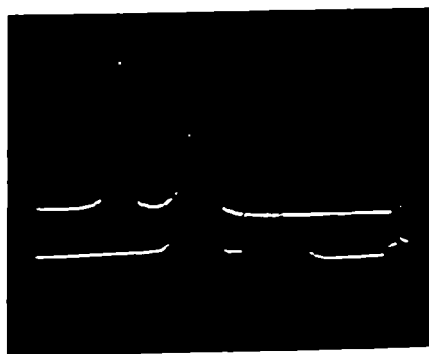


FIG. 21

is swept in succession across the collector slit. The current from the electron multiplier appears as negative peaks. These peaks are then amplified by a three-stage amplifier and thus appear as positive peaks of greater amplitude. The next circuit matches the height of the peaks, and displaces them by means of a small voltage added by a relay in the form of a 30-cycle square wave which is synchronized with the flipping voltage applied to the electrostatic analyser. The peaks are then displayed on the oscilloscope, which employs a 60-cycles/sec linear sweep. They appear one above the other, and can be matched horizontally by adjusting the flipping voltage on the electrostatic analyser. In practice, both members of the doublet may appear in each trace on the oscilloscope screen. This is shown in Fig. 19 and 21.

(vii) Accuracy of voltage measurements. The readings of ΔV were taken by means of a differential voltmeter (Fluke Mfg. Co. Model 801). Settings of ΔV were made by adjusting a helipot, and the voltages were read on the meter. The total voltage, V , across the electrostatic analyser was measured with the same meter. By considering the stated accuracy of the resistors in the differential voltmeter, it is possible to estimate errors in the voltages measured. The outside limit of error stated by the manufacturer is 0.05% for voltages above 0.1 volt, or 0.1 or 50 microvolts for voltages below 0.1 volt. However, voltage ratios, i.e. $\Delta V/V$, are more accurate than absolute determinations.

It is estimated that the accuracy of the ratio of two different voltages would be, at worst, 0.025%, if both voltages were above 0.1 volt, while, if one of these voltages were below 0.1 volt but above 0.01 volt, the error in the ratio would be, at worst, 0.03%. Many readings were made by adjusting a helipot, and the voltages were read on the meter.

(viii) Resolution attained. The expression for the resolution of this particular mass spectrometer, calculated from equation 11, is simply:

$$\Delta M/M = S/a_e$$

where S is the sum of the widths of the initial and final beam defining slits. Under typical operating conditions, S_1 was 0.0025 in. and S_4 was 0.003 in. This gives a theoretical resolution, for separation of peak bases, of 1/20,000. The best resolution (at the base of the peaks) obtained experimentally was about 1/18,000. If the criterion for resolution is the width of the peak at half maximum, then this figure is about 1/36,000.

It was found that the closing of S_4 beyond 0.003 in. did not improve the resolution achieved. This could be caused by a slight misalignment of S_1 and S_4 , which could not be easily checked because of the size and method of construction of the instrument. It is hoped that future improvements will make possible better alignment of these slits.

CHAPTER III

RESULTS OBTAINED AND DISCUSSION

1. Summary of Mass Difference Determinations

Table I shows the mass differences calculated from doublet measurements made during this investigation. Values obtained by others are shown for comparison.

TABLE I
Mass Difference Values in mMU

Doublet	(This work)	(Earlier Work)
$N_2O - CO_2$	11.2390 \pm 30	11.244 \pm 10 (a)
		11.2355 \pm 6* (b)
		11.23788 \pm 32 (c)
$N_2O - \frac{1}{2} Sr^{88}$	48.240 \pm 12	
$CO_2 - \frac{1}{2} Sr^{88}$	36.999 \pm 9	37.00 \pm 18 (d)
$C_3H_7 - \frac{1}{2} Sr^{86}$	100.126 \pm 25	100.12 \pm 5** (e)
$\frac{1}{2}(Zr^{90}Cl_2^{35}) - Kr^{80}$	4.9484 \pm 25	

* Actual doublet observed was $N_2 - CO$.

** " " " " $C_6H_{14} - Sr^{86}$

- (a) Kerr and Duckworth, 1958
- (b) Scolman, Quisenberry and Nier, 1956
- (c) Smith, 1958
- (d) Duckworth, Woodcock and Preston, 1951
- (e) Collins, Johnson and Nier, 1954.

The probable errors quoted are made up of a combination of the statistical error calculated in the usual way from the spread of the

readings, and an estimate of the precision of the voltage measurement. Only in the first and last doublets listed is the statistical error large enough to contribute to the total error.

The $N_2O - CO_2$ doublet was observed on four occasions over a period of nine days. The change in its determined value over this period was not significant compared with the accuracy of the voltage measurements.

2. New Mass Values Directly Calculated from These Differences

In determining the masses of Sr^{86} , Sr^{88} and Zr^{90} , the following masses were adopted.

$$C^{12} = 12.0038156 \pm 4 \quad (\text{Quisenberry, Giese and Benson, 1957})$$

$$H^1 = 1.0081451 \pm 2 \quad (\quad " \quad " \quad " \quad " \quad ")$$

$$Kr^{80} = 79.94177 \pm 10 \quad (\text{Duckworth, 1957})$$

$$Cl^{35} = 34.9799720 \pm 22 \quad (\text{Giese and Benson, 1957})$$

Table II shows the values obtained in this investigation and by others for comparison.

TABLE II

Nuclide	New Mass Values in Atomic Mass Units	
	This work	Others
N ¹⁴	14.0075273 ± 15	14.0075263 ± 7 (a)
		14.00752658 ± 9 (b)
Sr ⁸⁶	85.93667 ± 5	85.93648 ± 10 (c)
		85.9362 ± 8 (d)
Sr ⁸⁸	87.933634 ± 18	87.93396 ± 11 (c)
		87.93364 ± 36 (d)
Zr ⁹⁰	89.93350 ± 20*	89.93292 ± 25 (c)
		89.93295 ± 36 (e)

*This error is almost entirely due to the uncertainty in the mass of Kr-80, which served as the comparison mass.

- (a) Scolman, Quisenberry and Nier, 1956
- (b) Smith, 1958
- (c) Collins, Johnson and Nier, 1954
- (d) Duckworth, Woodcock and Preston, 1951
- (e) Duckworth, Preston and Woodcock, 1950

3. Comparison with Mass Differences from Nuclear Reaction Data

In the past there has been disagreement between mass spectroscopic values and nuclear disintegration data in the strontium and zirconium region of the atomic mass table (Duckworth, 1957).

It was partly the purpose of this investigation to attempt to resolve these difficulties. Fig. 22 shows some of the nuclides in this region and the Q values of nuclear reactions connecting adjacent nuclides.

FIGURE 22

NUCLIDIC CHART IN THE 50-NEUTRON REGION SHOWING REACTION Q-VALUES

References

- (a) Axel and Fox, 1956
- (b) Harvey, 1951
- (c) Shore, Bendel, Brown and Becker, 1953.
- (d) Moreau and Jorba, 1952.
- (e) Langer and Price, 1949.
- (f) Laslett, Jensen and Pasken, 1950.
- (g) Brown and Katcoff, 1949.
- (h) Chidley, Katz and Kowalski, 1958.
- (j) Bartholomew, Campion, Knowles and Manning, 1958.
- (k) Wall, 1954.
- (m) Stirling and Goldberg, 1956.
- (n) Bisi, Terrani and Zappa, 1955.
- (p) Way, King, McGinnis and van Lieshout, 1955.
- (r) McFarland and Shull, 1953.
- (s) Holt and Marsham. 1953.
- (t) Johnson, Johnson and Langer, 1955.
- (u) Pohn, Waddell and Jensen, 1956.

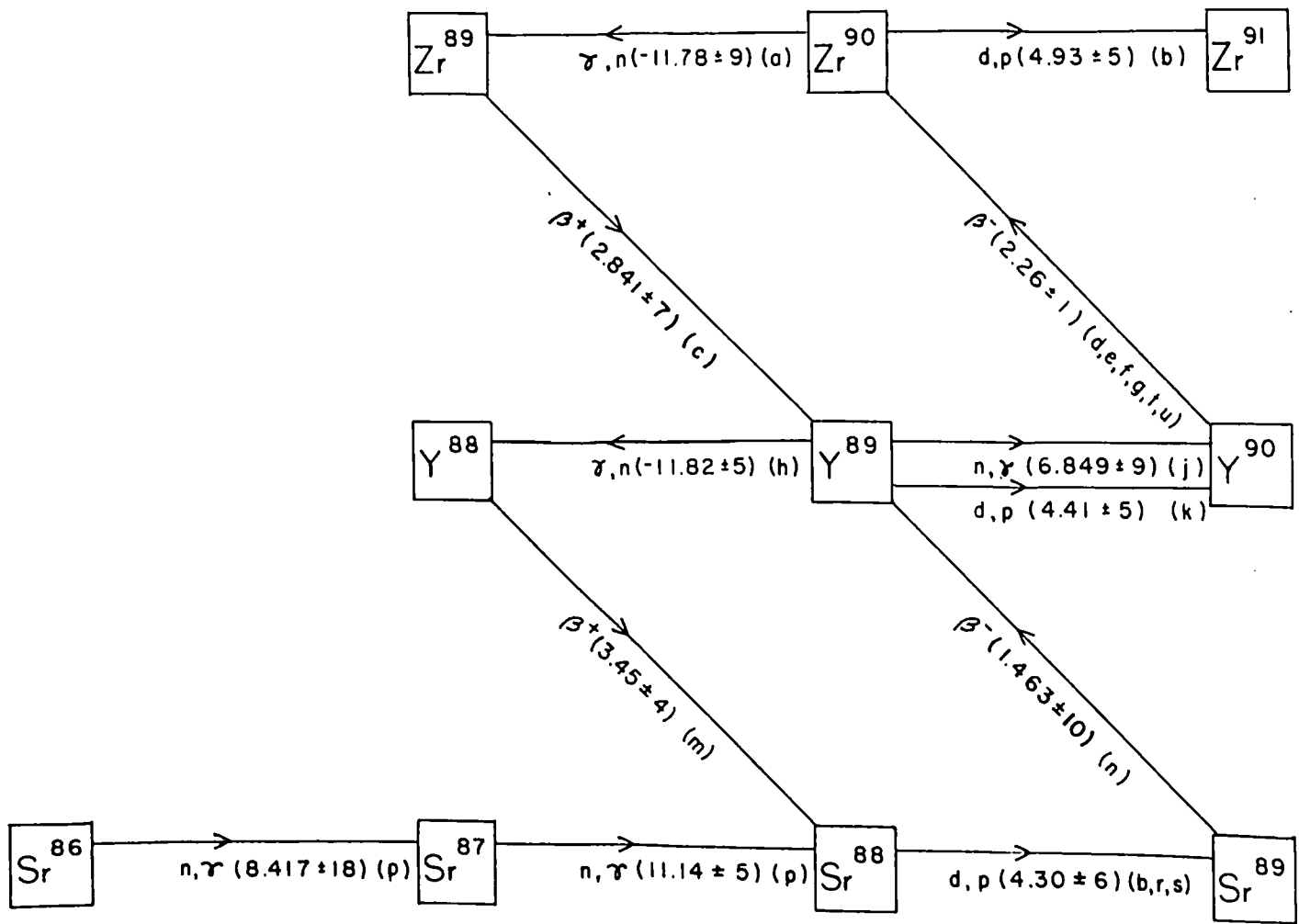


FIG. 22

(i) The $\text{Sr}^{88} - \text{Sr}^{86}$ Mass Difference. The Q values of $\text{Sr}^{86}(n, \gamma)\text{Sr}^{87}$ and $\text{Sr}^{87}(n, \gamma)\text{Sr}^{88}$ have been published (Way, 1955). The results are compared with mass spectroscopic data in Table III.

TABLE III

$\text{Sr}^{88} - \text{Sr}^{86}$ Mass Difference, Atomic Mass Units	
Transmutation data (Way, 1955)	1.99698 \pm 6
Mass spectroscopic data (Collins, Johnson and Nier, 1954)	1.99748 \pm 15
Mass spectroscopic data (Duckworth, Woodcock and Preston, 1951)	1.9974 \pm 9
Mass spectroscopic data (This work)	1.99696 \pm 5

The results of this investigation agree very well with the n , measurements. The results of previous best mass determinations disagree by about 0.5 mAU.

(ii) The $\text{Zr}^{90} - \text{Sr}^{88}$ Mass Difference. This difference can be obtained from nuclear reaction Q -values via various routes. Table IV gives these differences and compares them with the results of this work and other mass spectroscopic data.

TABLE IV
 $Zr^{90} - Sr^{88}$ Mass Difference

Route	Value, in A.M.U.	Reference
$Sr^{88}(d,p)Sr^{89}(\beta^-)Y^{89}(d,p)Y^{90}(\beta^-)Zr^{90}$	1.99984 ± 8	See Fig. 22
$Sr^{88}(d,p)Sr^{89}(\beta^-)Y^{89}(n,\gamma)Y^{90}(\beta^-)Zr^{90}$	1.99961 ± 6	" " "
$Sr^{88}(d,p)Sr^{89}(\beta^-)Y^{89}; Zr^{90}(\gamma,n)Zr^{89}(\beta^+)Y^{89}$	1.99980 ± 12	" " "
$Y^{89}(\gamma,n)Y^{88}(\beta^+)Sr^{88}; Zr^{90}(\gamma,n)Zr^{89}(\beta^+)Y^{89}$	1.99939 ± 12	" " "
$Y^{89}(\gamma,n)Y^{88}(\beta^+)Sr^{88}; Y^{89}(d,p)Y^{90}(\beta^-)Zr^{90}$	1.99943 ± 8	" " "
$Y^{89}(\gamma,n)Y^{88}(\beta^+)Sr^{88}; Y^{89}(n,\gamma)Y^{90}(\beta^-)Zr^{90}$	1.99920 ± 7	" " "
Mass spectroscopic	1.99896 ± 27	Collins, Johnson and Nier, 1954.
" "	1.99931 ± 50	Duckworth, Preston and Woodcock, 1950, and Duckworth, Woodcock and Preston, 1951
" "	1.99987 ± 20	This work

The six transmutation values fall into two groups of three. The first three agree rather well with the mass difference calculated from the results of this investigation, while the last three are different by about 0.5 mAU.

The mass spectroscopic value for the mass difference $Zr^{90} - Sr^{88}$ calculated from the results of Collins, Johnson and Hicr (1954) is lower than all the transmutation results, and is lower than the value resulting from this work by 0.9 mAU. The value calculated from the older results of Duckworth has too large a probable error to make meaningful comparisons possible.

Transmutation data disagree regarding the mass difference $Y^{89} - Sr^{88}$. This gives rise to the two groups of values in Table IV. The two values are calculated from the reactions $Sr^{88}(d,p)Sr^{89}(\beta^-)Y^{89}$, and $Y^{89}(\gamma,n)Y^{88}(\beta^+)Sr^{88}$. The former gives $Y^{89} - Sr^{88} = 1.00041 \pm 6$ AMU, while the latter gives 1.00000 ± 7 AMU. The mass spectroscopic determinations resulting from this investigation agree with the first value.

This discrepancy of 0.41 in AU indicates that at least one of the four transmutation data is in error. Since the $Sr^{88}(d,p)Sr^{89}$, and the $Sr^{89}(\beta^-)Y^{89}$ results agree with the mass determinations reported here, it is reasonable to suspect either the $Y^{89}(\gamma,n)Y^{88}$ reaction or the $Y^{88}(\beta^+)Sr^{88}$ decay.

The $Y^{88}(\gamma,n)Y^{88}$ reaction was studied using a betatron (Chidley Katz and Kowalski, 1958) and observing the resulting neutrons directly, rather than observing the resulting Y^{88} activity.

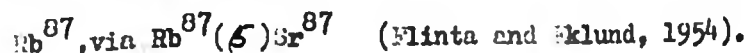
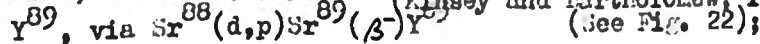
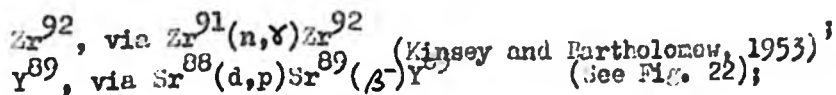
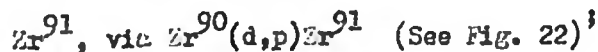
The plot of neutron counts versus betatron energy gives a rather definite threshold, and it seems quite certain that the ground state of Y^{86} was observed.

The Q -value of the Y^{88} decay was reported (Heacock and Jones, 1943) to be 3.70 Mev. or 3.97 mMU. This value is now considered to be too high (Sterling and Goldberg, 1956) by 0.25 MeV, or 0.27 mMU. Actually, the old Q -value gives better agreement with the other transmutation data and also with the mass values obtained in this investigation.

Quite aside from the results of these mass determinations, there exists a considerable discrepancy between the transmutation values for the mass difference $Y^{89} - Sr^{88}$. This matter deserves further attention from ^{beta ray} spectroscopists and nuclear reaction workers.

4. Other Mass Values Derived from this Investigation

Besides the mass values already listed, others may be calculated by combining transmutation data with the results of this work. Some of these are:



The results of these calculations are given in the summary of mass values under conclusions.

CONCLUSIONS

A new large double-focusing mass spectrometer has been developed to the stage where it is useful for the determination of precise atomic mass values. The precision of the mass comparisons that have been made with the instrument ranges from one part in 1.7×10^6 to one part in 3.2×10^7 . The errors in the less precise values are almost entirely due to the uncertainty in the voltmeter readings.

Direct determinations of the masses of N^{14} , Sr^{80} , Sr^{88} and Zr^{90} have been made. The three last-mentioned appear to resolve the serious discrepancies that have existed between mass spectroscopic and nuclear transmutation data for the $Sr^{86} - Sr^{88}$ and the $Zr^{90} - Sr^{88}$ mass differences.

New mass values have been determined for several other nuclides by combining the results of this work with existing transmutation Q -values.

The new mass values resulting from this work are listed in Table V.

TABLE V

New Atomic Mass Values Resulting
from this Work

Nuclide	Mass Value, in AMU
N ¹⁴	14.0075273 ± 15
Rb ⁸⁷	86.93691 ± 6
Sr ⁸⁶	85.93667 ± 5
Sr ⁸⁷	86.93662 ± 6
Sr ⁸⁸	87.933634 ± 18
Y ⁸⁹	88.93404 ± 6
Zr ⁹⁰	89.93350 ± 20
Zr ⁹¹	90.93480 ± 21
Zr ⁹²	91.93448 ± 21

REFERENCES

- Allen, J. S. 1947. Rev. Sci. Instrum. 18: 739.
- Aston, F. W. 1919. Phil. Mag. 38: 709.
- Axel, P. and Fox, J. D. 1956. Phys. Rev. 102: 400.
- Bainbridge, K. T. and Jordan, E. B. 1936. Phys. Rev.:50
- Bartholomew, G. A., Campion, F. J., Knowles, J. W., and Manning, G.
1958. Bull. Am. Phys. Soc. 11, 2: 828.
- Bisi, A., Terrani, S., and Zappa, L. 1955. Nuovo Cim. 2:1052.
- Bleakney, W. 1936. American Physics Teacher 4:12.
- Brown, L., and Katcoff, S. 1949. J. Chem. Phys. 17:505.
- Chidley, B. G., Katz, L., Kowalski, S. 1958. Can. J. Phys. 36:407.
- Collins, T. L., Johnson, W. H., and Mier, A. O. 1954. Phys. Rev. 94:
398.
- Dempster, A. J. 1935. Proc. Amer. Phil. Soc. 75:755.
- Dewdney, J. W. 1955. Ph.D. Dissertation, McMaster University.
- Duckworth, H. E. 1957. "Progress in Nuclear Physics" Vol.6, pp.138-161:
Pergamon Press.
- Duckworth, H. E., and Preston, R. S. 1951. Phys. Rev. 82:486.
- Duckworth, H. E., Preston, R. S., and Woodcock, K. S. 1950.
Phys. Rev. 72:180.
- Flinta, J., and Eklund, S. 1954. Arkiv. Fysik 7:401.
- Giese, C. F., and Benson, J. L. 1957. Bull. Am. Phys. Soc. 11
2:223
- Harvey, J. A. 1951. Phys. Rev. 81:355.
- Herzog, R. 1934. Zeits. Phys. 69:447.
- _____ 1935. Zeits. Phys. 27:596.
- Holt, J. R., and Marshall, T. N. 1953. Proc. Roy. Soc. (London)
66A:565.

- Johnson, O. E., Johnson, R. G., and Langer, L. M. 1955.
Phys. Rev. 98:1517.
- Kerr, J. T. 1957. Ph.D. Dissertation, McMaster University.
- Kerr, J. T. and Duckworth, H. E. 1958. Can. J. Phys. 36:986.
- Langer, L. M., and Price, H. C. 1949. Phys. Rev. 76, 136A,
454A. 641.
- Laslett, L. J., Jenson, E. N., and Paskin, A. 1950. Phys. Rev.
79:412.
- Mattauch, J., and Herzog, R. 1934. Zeits. Phys. 89:786.
- McFarland, C. E., and Shull, F. B. 1953. Phys. Rev. 89:692.
- Moreau, J., and Perez y Jorba. 1952. Compt. Rend. 235:39
- Peacock, W. C., and Jones, J. W. 1948. U. S. Atomic Energy
Commission AECU-1812.
- Fohm, A. V., Maddell, R. C., and Jensen, E. M. 1956.
Phys. Rev. 101:1067.
- Quisenberry, K. S., Giese, C. F., and Bensen, J. L. 1957.
Bull. Am. Phys. Soc. II, 2:223.
- Quisenberry, K. S., Scolman, T. T., and Nier, A. O. 1956.
Phys. Rev. 102: 1076.
- Scolman, T. T., Quisenberry, K. S., and Nier, A. O. 1956.
Phys. Rev. 102: 1076
- Shore, F. J., Wendel, W. L., Brown, H. N., and Becker, R. A.
1953. Phys. Rev. 91:1203.
- Smith, L. G. 1951. Phys. Rev. 81:295.
- _____ 1958. Phys. Rev. 111:1606.
- Smith, L. G., and Damm, C. C. 1956. Rev. Sci. Instrum. 27:638.
- Stirling, W. L., and Goldberg, N. 1956. Bull. Am. Phys. Soc. II,
1:291.
- Wall, N. S. 1954. Phys. Rev. 96: 664.
- Way, K., King, R. W., McGinnis, C. L. and van Lieshout, R. 1955.
"Nuclear Level Schemes," U. S. Atomic Energy Commission TID-5300.

- Johnson, O. E., Johnson, R. G., and Langer, L. H. 1955.
Phys. Rev. 98:1517.
- Kerr, J. T. 1957. Ph.D. Dissertation, McMaster University.
- Kerr, J. T. and Duckworth, H. E. 1958. Can. J. Phys. 36:986.
- Langer, L. H., and Price, H. C. 1949. Phys. Rev. 76, 136A,
454A. 641.
- Laslett, L. J., Jenson, E. N., and Paskin, A. 1950. Phys. Rev.
79:412.
- Mattauch, J., and Herzog, R. 1934. Zeits. Phys. 89:786.
- McFarland, C. E., and Shull, F. B. 1953. Phys. Rev. 89:892.
- Moreau, J., and Perez y Jorba. 1952. Compt. Rend. 235:39
- Peacock, W. C., and Jones, J. W. 1948. U. S. Atomic Energy
Commission AECU-1812.
- Pohm, A. V., Maddell, B. C., and Jonsen, E. N. 1956.
Phys. Rev. 101:1067.
- Quisenberry, K. S., Giese, C. F., and Bensen, J. L. 1957.
Bull. Am. Phys. Soc. II, 2:223.
- Quisenberry, K. S., Scolman, T. T., and Nier, A. O. 1956.
Phys. Rev. 102. 1076.
- Scolman, T. T., Quisenberry, K. S., and Nier, A. O. 1956.
Phys. Rev. 102: 1076
- Shore, F. J., Bendel, W. L., Brown, H. H., and Becker, R. A.
1953. Phys. Rev. 91:1203.
- Smith, L. G. 1951. Phys. Rev. 81:295.
- _____ 1958. Phys. Rev. 111:1606.
- Smith, L. G., and Damm, C. C. 1956. Rev. Sci. Instrum. 27:638.
- Stirling, W. L., and Goldberg, N. 1956. Bull. Am. Phys. Soc. II,
1:291.
- Wall, N. S. 1954. Phys. Rev. 96: 664.
- Way, K., King, R. W., McCinnis, C. L. and van Lieshout, N. 1955.
"Nuclear Level Schemes," U. S. Atomic Energy Commission TID-5300.